

(This is a sample cover image for this issue. The actual cover is not yet available at this time.)

This article appeared in a journal published by Elsevier. The attached copy is furnished to the author for internal non-commercial research and education use, including for instruction at the authors institution and sharing with colleagues.

Other uses, including reproduction and distribution, or selling or licensing copies, or posting to personal, institutional or third party websites are prohibited.

In most cases authors are permitted to post their version of the article (e.g. in Word or Tex form) to their personal website or institutional repository. Authors requiring further information regarding Elsevier's archiving and manuscript policies are encouraged to visit:

<http://www.elsevier.com/copyright>

Contents lists available at [SciVerse ScienceDirect](#)

Journal of Theoretical Biology

journal homepage: www.elsevier.com/locate/jtbi

On the biomechanics and mechanobiology of growing skin

Alexander M. Zöllner^a, Adrian Buganza Tepole^a, Ellen Kuhl^{a,b,c,d,*}^a Department of Mechanical Engineering, Stanford University, Stanford, CA 94305, USA^b Department of Mechanical and Process Engineering, Center of Mechanics, ETH Zurich, 8092 Zurich, Switzerland^c Department of Bioengineering, Stanford University, Stanford, CA 94305, USA^d Department of Cardiothoracic Surgery, Stanford University, Stanford, CA 94305, USA

ARTICLE INFO

Article history:

Received 29 October 2011

Received in revised form

6 December 2011

Accepted 21 December 2011

Available online 4 January 2012

Keywords:

Skin

Biological membranes

Mechanotransduction

Growth

Tissue expansion

ABSTRACT

Skin displays an impressive functional plasticity, which allows it to adapt gradually to environmental changes. Tissue expansion takes advantage of this adaptation, and induces a controlled *in situ* skin growth for defect correction in plastic and reconstructive surgery. Stretches beyond the skin's physiological limit invoke several mechanotransduction pathways, which increase mitotic activity and collagen synthesis, ultimately resulting in a net gain in skin surface area. However, the interplay between mechanics and biology during tissue expansion remains unquantified. Here, we present a continuum model for skin growth that summarizes the underlying mechanotransduction pathways collectively in a single phenomenological variable, the strain-driven area growth. We illustrate the governing equations for growing biological membranes, and demonstrate their computational solution within a nonlinear finite element setting. In displacement-controlled equi-biaxial extension tests, the model accurately predicts the experimentally observed histological, mechanical, and structural features of growing skin, both qualitatively and quantitatively. Acute and chronic elastic uniaxial stretches are 25% and 10%, compared to 36% and 10% reported in the literature. Acute and chronic thickness changes are –28% and –12%, compared to –22% and –7% reported in the literature. Chronic fractional weight gain is 3.3, compared to 2.7 for wet weight and 3.3 for dry weight reported in the literature. In two clinical cases of skin expansion in pediatric forehead reconstruction, the model captures the clinically observed mechanical and structural responses, both acutely and chronically. Our results demonstrate that the field theories of continuum mechanics can reliably predict the mechanical manipulation of thin biological membranes by controlling their mechanotransduction pathways through mechanical overstretch. We anticipate that the proposed skin growth model can be generalized to arbitrary biological membranes, and that it can serve as a valuable tool to virtually manipulate living tissues, simply by means of changes in the mechanical environment.

© 2011 Elsevier Ltd. All rights reserved.

1. Introduction

Human skin is a remarkable organ that can be stretched to manyfold its original size, while remaining phenotypically similar to its initial state, without any reported malignant transformation (Beauchenne et al., 1989; De Filippo and Atala, 2002). To enable this incredible expansion, skin is a highly specialized mechanoresponsive interface, characterized through a network of interrelated cascades involving extracellular, membrane, cytosolic, cytoskeletal, and nuclear mechanisms (Silver et al., 2003). When skin is stretched

beyond its physiological limit, these mechanisms act in concert to restore the homeostatic equilibrium state. In this regulatory process, transmembrane mechanosensors in the form of stretch-activated ion channels, integrins, growth factor receptors, and G-protein-coupled receptors play a key role in translating extracellular events into intracellular signals (Jaaloul and Lammerding, 2009; Wong et al., 2011), see Fig. 1.

Stretch-activated ion channels open in response to elevated membrane strains, allowing positively charged calcium ions (Ca^{2+}) and other cations to enter the cell. Changes in the intracellular calcium concentration are known to regulate intracellular signaling and cytoskeletal remodeling (Silver et al., 2003). Integrins are receptors that mediate attachment between a cell and the extracellular matrix (Simpson et al., 2011). They play a central role in force transmission across the cell membrane, triggering targets such as nitric oxide (NO) signaling, mitogen-associated protein kinases (MAPK), Rho GTPases, and phosphoinositol-3-kinase (PI3K). Growth

* Corresponding author at: Department of Mechanical Engineering, Stanford University, 496 Lomita Mall, Stanford, CA 94305, USA. Tel.: +1 650 450 0855; fax: +1 650 725 1587.

E-mail addresses: azoell@stanford.edu (A.M. Zöllner), abuganza@stanford.edu (A. Buganza Tepole), ekuhl@stanford.edu (E. Kuhl).
URL: <http://biomechanics.stanford.edu> (E. Kuhl).

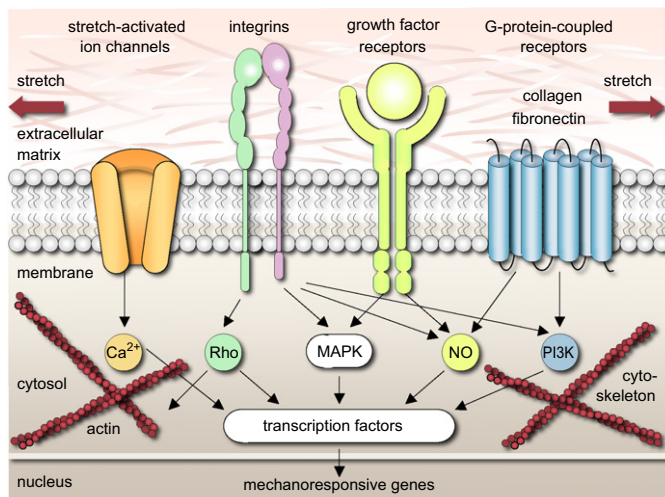


Fig. 1. Mechanotransduction of growing skin. Transmembrane mechanosensors in the form of stretch-activated ion channels, integrins, growth factor receptors, and G-protein-coupled receptors translate extracellular signals into intracellular events, which activate a cascade of interconnected signaling pathways. Biomechanical and biochemical signals converge in the activation of transcription factors, activating gene expression. Mechanotransduction triggers increased mitotic activity and increased collagen synthesis, resulting in an increase in skin surface area to restore the homeostatic equilibrium state (Jaalouk and Lammerding, 2009; Wong et al., 2011).

factor receptors bind to growth factors outside the cell, thereby turning on several receptor mediated pathways inside the cell, such as nitric oxide (NO) signaling and mitogen-associated protein kinases (MAPK) (Jaalouk and Lammerding, 2009). Mitogen-associated protein kinase signaling pathways convey information to effectors, coordinate incoming information from other signaling cascades, amplify signals, and initiate a variety of response patterns. G-protein-coupled receptors are seven-transmembrane proteins, which can potentially be activated by mechanical stretch outside the cell to initiate mechanotransduction pathways inside the cell through second messengers such as nitric oxide (NO) signaling and phosphoinositide-3-kinase (PI3K). Last, intracellular strain can induce conformational changes in the cytoskeleton itself. These changes may affect the binding affinities to specific molecules and thereby activate additional signaling pathways (Langevin et al., 2005).

In summary, mechanical activation initiates multiple signaling pathways, which can have a substantial overlap and crosstalk. However, since mechanically induced signaling pathways may be shared with classical receptor-mediated pathways, they are typically difficult to study in isolation. It is clear, however, that all these signaling pathways converge to activate transcription factors, which stimulate gene expression and other nuclear events (Wong et al., 2011). Overall, the underlying principle is that stretch invokes a cascade of events that trigger increased mitotic activity and increased collagen synthesis, which ultimately result in increased skin surface area to restore the homeostatic equilibrium state (Takei et al., 1998).

Taking advantage of mechanotransduction is a powerful approach to endogenously engineer new skin. Since it was first introduced in the mid 1950s (Neumann, 1959), the controlled mechanical manipulation of skin has opened a whole new frontier in reconstructive surgery. Today tissue expansion is widely used to repair birth defects (Arneja and Gosain, 2007), correct burn injuries (Argenta et al., 1983), and reconstruct breasts after tumor removal (Radovan, 1982). It is the ideal strategy to grow skin that matches the color, texture, hair bearing, and thickness of the surrounding healthy skin, while minimizing scars and risk of rejection (Rivera et al., 2005).

Tissue expansion is an iterative procedure of controlled overstretch, progressive skin growth, and gradual restoration of the homeostatic equilibrium state, repeated in several weekly intervals (Gosain et al., 2001). To grow skin in a desired location, the surgeon dissects a subcutaneous pocket between the dermis and the hypodermis (Gosain et al., 2009), in which he places the expander. The expander is successively filled with saline solution by a remote injection port, see Fig. 2. By visual inspection of skin color, capillary refill, and palpation of the expanded skin, the surgeon heuristically determines the amount of filling (Rivera et al., 2005). Once enough new skin is produced, typically after a period of multiple weeks, the device is removed, and the new skin is used to repair the adjacent defect zone. Although tissue expansion is a common surgical procedure today, there are no scientific guidelines for optimal device selection. Accordingly, the appropriate choice of expander shape, expander size, expander location, filling volume, and filling timing remains almost exclusively based on the surgeon's experience and personal preference (LoGiudice and Gosain, 2003).

The first quantitative model for growing skin was proposed only a few years ago, and has unfortunately not received a lot of attention to date (Socci et al., 2007). Motivated by this first study on axisymmetric skin growth, conceptually similar to an axisymmetric model for growing cell walls (Goriely and Tabor, 2003), we have recently established a prototype model for growing biological membranes to predict skin growth in a general three-dimensional setting (Buganza Tepole et al., 2011). The model is based on the continuum framework of finite growth (Rodriguez et al., 1994), originally developed for the isotropic volumetric growth of biological solids (Ambrosi and Mollica, 2002; Epstein and Maugin, 2000; Lubarda and Hoger, 2002). Its key kinematic feature is the multiplicative decomposition of the deformation gradient into a reversible elastic part and an irreversible growth part (Garikipati, 2009; Lubarda, 2004), a concept that was adopted from finite plasticity (Lee, 1969). Over the past decade, continuum growth theories have been rapidly developed and intensely refined to characterize isotropic (Ciarletta and Ben Amar, in press; Goriely and Ben Amar, 2007; Kuhl et al., 2007), transversely isotropic (Rausch et al., 2011; Taber, 1995), orthotropic (Göktepe et al., 2010b; Taber and Eggers, 1996), and generally anisotropic (Ambrosi et al., 2010; Menzel, 2007) growth phenomena, both compressibly (McMahon and Goriely, 2010) and incompressibly (Humphrey, 2002; Schmid et al., 2011).

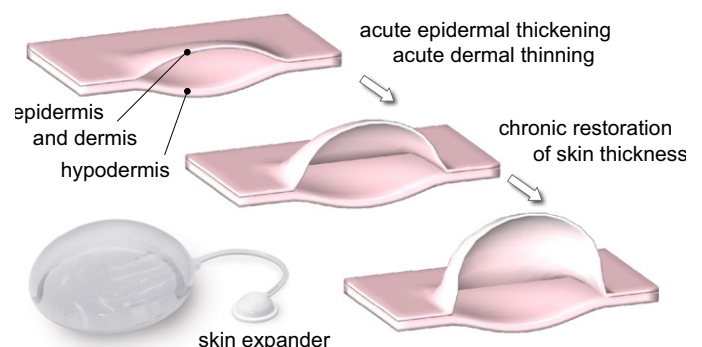


Fig. 2. Biomechanics of growing skin. At biological equilibrium, the skin is in a homeostatic state of resting tension. To grow skin for defect repair, a tissue expander is placed in a subcutaneous pocket underneath the epidermis and the dermis, above the hypodermis. When the expander is inflated, the skin is stretched, associated with an acute dermal thinning attributed to the Poisson effect. Stretches beyond a critical level trigger a series of signaling pathways leading to the creation of new skin. Skin restores its homeostatic state, associated with the chronic restoration of the original thickness. Upon expander removal, elastic deformations retract and inelastic deformations remain.

Recent trends focus on the computational modeling of finite growth (Ambrosi et al., 2011; Himpel et al., 2005), typically by introducing the growth tensor as an internal variable within a nonlinear finite element framework (Göktepe et al., 2010a; Kroon et al., 2009), a strategy that we also adopt here. To predict the biomechanics and mechanobiology of growing skin and their impact on stress, strain, and area gain, we adopt a transversely isotropic growth model (Buganza Tepole et al., 2011, in press), in which all cellular and molecular mechanisms are collectively summarized in a single phenomenological internal variable, the in-plane area growth. Here, in contrast to our previous model formulated in the material frame of reference (Zöllner et al., in press), we introduce a spatial formulation, which lends itself to a computationally elegant and highly efficient algorithm. To simulate heterogeneous growth phenomena on anatomically realistic geometries, we integrate the growth model into a multi-purpose nonlinear finite element program (Taylor, 2008). We illustrate its features by means of the simple model problem of equi-biaxial extension and through two clinical cases of skin expansion in pediatric forehead reconstruction.

2. Methods

2.1. Continuum model of growing skin

To accurately represent the finite deformations during skin expansion, we adopt the kinematics of finite growth, and introduce the deformation map ϕ , which, at any given time t , maps the material placement \mathbf{X} of a physical particle onto its spatial placement $\mathbf{x} = \phi(\mathbf{X}, t)$. We then introduce the multiplicative decomposition of the deformation gradient (Rodriguez et al., 1994)

$$\mathbf{F} = \nabla_{\mathbf{x}} \phi = \mathbf{F}^e \cdot \mathbf{F}^g \quad (1)$$

into a reversible elastic part \mathbf{F}^e and an irreversible growth part \mathbf{F}^g , in agreement with experimental findings (van Rappard et al., 1988). Here, $\nabla\{\circ\} = \partial_{\mathbf{x}}\{\circ\}|_t$ denotes the gradient of a field $\{\circ\}(\mathbf{X}, t)$ with respect to the material placement \mathbf{X} at fixed time t . Its Jacobian defines the overall change in tissue volume

$$J = \det(\mathbf{F}) = J^e J^g \quad (2)$$

which we can equivalently decompose into a reversibly elastic volume change $J^e = \det(\mathbf{F}^e)$ and an irreversibly grown volume change $J^g = \det(\mathbf{F}^g)$. Skin is a composite material consisting of a 0.1–1.0 mm thick, waterproof, protective outer layer, the epidermis, and a 1.0–4.0 mm thick, load bearing inner layer, the dermis (Silver et al., 2003), which we idealize jointly as a single layer. We characterize its area stretch through Nanson's formula

$$\mathcal{A} = \|\text{cof}(\mathbf{F}) \cdot \mathbf{n}_0\| = \mathcal{A}^e \mathcal{A}^g \quad (3)$$

in terms of the skin plane normal \mathbf{n}_0 in the undeformed reference configuration, where $\text{cof}(\circ) = \det(\circ)(\circ)^{-t}$ denotes the cofactor of a second order tensor (\circ) . The area stretch obeys the multiplicative decomposition into a reversibly elastic area stretch \mathcal{A}^e and an irreversibly grown area stretch $\mathcal{A}^g = \|\text{cof}(\mathbf{F}^g) \cdot \mathbf{n}_0\|$. To model stretch-induced skin growth, we collectively summarize the effects of mechanotransduction in a single scalar-valued variable \mathcal{A}^g , which characterizes the evolution of the in-plane area growth, while the response in the thickness direction \mathbf{n}_0 is assumed to be purely elastic (Beauchenne et al., 1989). Accordingly, we can express the growth tensor \mathbf{F}^g in the following simple format:

$$\mathbf{F}^g = \sqrt{\mathcal{A}^g} \mathbf{I} + [1 - \sqrt{\mathcal{A}^g}] \mathbf{n}_0 \otimes \mathbf{n}_0 \quad (4)$$

Since the material is not assumed to grow in the thickness direction \mathbf{n}_0 (Rivera et al., 2005; van der Kolk et al., 1987), its area growth is

identical to its volume growth, i.e., $\mathcal{A}^g = \det(\mathbf{F}^g) = J^g$. Using the simple rank-one update structure of \mathbf{F}^g , we can apply the Sherman–Morrison formula to invert the growth tensor explicitly

$$\mathbf{F}^{g-1} = \frac{1}{\sqrt{\mathcal{A}^g}} \mathbf{I} + \left[1 - \frac{1}{\sqrt{\mathcal{A}^g}}\right] \mathbf{n}_0 \otimes \mathbf{n}_0 \quad (5)$$

and obtain an explicit representation of the elastic tensor \mathbf{F}^e

$$\mathbf{F}^e = \frac{1}{\sqrt{\mathcal{A}^g}} \mathbf{F} + \left[1 - \frac{1}{\sqrt{\mathcal{A}^g}}\right] \mathbf{n} \otimes \mathbf{n}_0 \quad (6)$$

in terms of the spatial normal $\mathbf{n} = \mathbf{F} \cdot \mathbf{n}_0$. From the push forward of the contravariant material and intermediate metric tensors \mathbf{G}^{-1} and \mathbf{G}^{g-1} , we obtain the left Cauchy Green tensor $\mathbf{b} = \mathbf{F} \cdot \mathbf{G}^{-1} \cdot \mathbf{F}^t$ and its counterpart \mathbf{b}^e in the deformed, current configuration

$$\mathbf{b}^e = \mathbf{F}^e \cdot \mathbf{G}^{g-1} \cdot \mathbf{F}^{et} = \frac{1}{\mathcal{A}^g} \mathbf{b} + \left[1 - \frac{1}{\mathcal{A}^g}\right] \mathbf{n} \otimes \mathbf{n} \quad (7)$$

To focus on the impact of growth, we assume skin to behave isotropically elastic within the in vivo loading range of interest. Accordingly, we introduce the following Helmholtz free energy:

$$\psi = \frac{1}{2} \lambda \ln^2(J^e) + \frac{1}{2} \mu [\mathbf{g} : \mathbf{b}^e - 3 - 2 \ln(J^e)] \quad (8)$$

to evaluate the standard dissipation inequality, which defines the Kirchhoff stress $\boldsymbol{\tau}$ as thermodynamically conjugate to covariant spatial metric \mathbf{g}

$$\boldsymbol{\tau} = 2 \frac{\partial \psi}{\partial \mathbf{g}} = [\lambda \ln(J^e) - \mu] \mathbf{g}^{-1} + \mu \mathbf{b}^e \quad (9)$$

This implies that the newly created skin will have the same microstructure, density, and stiffness, as the original, native tissue (Beauchenne et al., 1989; Buganza Tepole et al., 2011). We model skin growth as a strain-driven process (Gosain et al., 2009), and introduce the following evolution equation for the area growth:

$$\dot{\mathcal{A}}^g = k^g(\mathcal{A}^g) \phi^g(\mathcal{A}^e) \quad (10)$$

in which $k^g(\mathcal{A}^g)$ is a weighting function and $\phi^g(\mathcal{A}^e)$ is a growth criterion similar to a yield function in the theory of plasticity. For the weighting function, we adopt a well-established functional form (Lubarda and Hoger, 2002), which we rephrase here in a strain-driven format (Göktepe et al., 2010a,b), to control unbounded growth

$$k^g = \frac{1}{\tau} \left[\frac{\mathcal{A}^{\max} - \mathcal{A}^g}{\mathcal{A}^{\max} - 1} \right]^\gamma \quad (11)$$

The adaptation speed τ and the shape parameter for the adaptation curve γ control the speed of adaptation, whereas the maximum area growth \mathcal{A}^{\max} defines the biological equilibrium state (Himpel et al., 2005; Lubarda and Hoger, 2002). For the growth criterion, we assume that growth is driven by the elastic area stretch \mathcal{A}^e

$$\phi^g = \langle \mathcal{A}^e - \mathcal{A}^{\text{crit}} \rangle = \langle \mathcal{A} / \mathcal{A}^g - \mathcal{A}^{\text{crit}} \rangle \quad (12)$$

and that it is activated only if the elastic area stretch exceeds a critical physiological limit $\mathcal{A}^{\text{crit}}$, where $\langle \circ \rangle$ denote the Macaulay brackets.

2.2. Computational model of growing skin

To solve the nonlinear finite element equations of stretch-induced skin growth, we implement the growth model in a custom-designed version of the multi-purpose nonlinear finite element program FEAP (Taylor, 2008). To characterize the growth process at each instant in time, we introduce the area growth \mathcal{A}^g as an internal variable, and solve the biological equilibrium equation (10) locally at the integration point level. At each discrete time step t , we determine the current area growth \mathcal{A}^g for a given current deformation state \mathbf{F} and a given area growth \mathcal{A}_n^g

from the previous time step t_n . Accordingly, we introduce the following finite difference approximation for the material time derivative of the area growth:

$$\dot{\mathcal{G}}^g = [\mathcal{G}^g - \mathcal{G}_n^g] / \Delta t \quad (13)$$

where $\Delta t = t - t_n$ denotes the current time increment. In the spirit of implicit time stepping schemes, we now reformulate the evolution equation (10) with the help of Eq. (13), introducing the discrete residual R^g in terms of the unknown area growth \mathcal{G}^g

$$R^g = \mathcal{G}^g - \mathcal{G}_n^g - k^g \phi^g \Delta t \doteq 0 \quad (14)$$

We solve this nonlinear equation using a local Newton iteration. Within each iteration step, we calculate the linearization of the residual R^g with respect to the area growth \mathcal{G}^g

$$K^g = \frac{\partial R^g}{\partial \mathcal{G}^g} = 1 - \left[\frac{\partial k^g}{\partial \mathcal{G}^g} \phi^g + k^g \frac{\partial \phi^g}{\partial \mathcal{G}^g} \right] \Delta t \quad (15)$$

in terms of the linearizations of the weighting function $\partial k^g / \partial \mathcal{G}^g = -\gamma k^g / [\mathcal{G}^{\max} - \mathcal{G}^g]$ and the growth criterion $\partial \phi^g / \partial \mathcal{G}^g = -\mathcal{G}^g / \mathcal{G}^{g2}$ introduced in Eqs. (11) and (12). We update the unknown area growth iteratively

$$\mathcal{G}^g \leftarrow \mathcal{G}^g - R^g / K^g \quad (16)$$

until we achieve convergence, i.e., until the absolute value of the local growth update $\Delta \mathcal{G}^g = -R^g / K^g$ is below a user-defined threshold value. Once we have iteratively determined the current area growth \mathcal{G}^g , we can successively determine the growth tensor F^g from Eq. (4), the elastic tensor $F^e = F \cdot F^g^{-1}$ from Eq. (6), the Kirchhoff stress τ from Eq. (9), and, finally, the fourth order tensor e of the Eulerian constitutive moduli

$$e = 2 \frac{d\tau}{dg} = e^e + e^g = 2 \frac{\partial \tau}{\partial g} \bigg|_{F^g} + \frac{\partial \tau}{\partial \mathcal{G}^g} \otimes 2 \frac{\partial \mathcal{G}^g}{\partial g} \bigg|_F \quad (17)$$

The first term, the partial derivative of the Kirchhoff stress τ with respect to the covariant spatial metric g , defines elastic constitutive moduli $e^e = 2 \partial \tau / \partial g$

$$2 \frac{\partial \tau}{\partial g} = \lambda g^{-1} \otimes g^{-1} + [\mu - \lambda \ln(J^e)] [g^{-1} \otimes g^{-1} + g^{-1} \otimes g^{-1}] \quad (18)$$

where we have used the common abbreviations, $\{\bullet \otimes \otimes\}_{ijkl} = \{\bullet\}_{ik} \{\bullet\}_{jl}$ and $\{\bullet \otimes \otimes\}_{ijkl} = \{\bullet\}_{il} \{\bullet\}_{jk}$, for the non-standard fourth order products. The second term

$$\frac{\partial \tau}{\partial \mathcal{G}^g} = -\frac{1}{\mathcal{G}^{g2}} [\lambda \mathcal{G}^g g^{-1} + \mu [b - n \otimes n]] \quad (19)$$

depends directly on the constitutive formulation for the Kirchhoff stress τ in Eq. (9) and indirectly on the particular format of the growth tensor F^g in Eq. (4). The third term

$$2 \frac{\partial \mathcal{G}^g}{\partial g} = \frac{1}{\tau} \frac{1}{\mathcal{G}^g} \left[\frac{\mathcal{G}^{\max} - \mathcal{G}^g}{\mathcal{G}^{\max} - 1} \right]^\gamma \frac{1}{K^g} \Delta t \times \left[\mathcal{G}^g g^{-1} - \frac{J^2}{\mathcal{G}^g} [F^{-t} \cdot n_0] \otimes [F^{-t} \cdot n_0] \right] \quad (20)$$

consists of the algorithmic linearization of the time discrete evolution equation for the area growth $\partial \mathcal{G}^g / \partial \mathcal{G}$ in Eq. (16) and of the linearization of the area stretch $2 \partial \mathcal{G} / \partial g$ in Eq. (3). The local stress of Eq. (9) and the local consistent tangent of Eq. (17) enter the global right-hand side vector and the global iteration matrix of the global Newton iteration. Upon its convergence, we store the corresponding area growth \mathcal{G}^g locally at the integration point level.

3. Results

We illustrate the features of the proposed growth model for the simple model problem of displacement-driven equi-biaxial extension and for the clinical case of tissue expansion in pediatric

forehead reconstruction. For the elastic model, we assume Lamé constants of $\lambda = 0.7141$ MPa and $\mu = 0.1785$ MPa, which would correspond to Young's modulus of $E = 0.5$ MPa and Poisson's ratio of $\nu = 0.4$ in the linear regime (Agache et al., 1980; Serup et al., 2003). For the growth model, we assume that growth takes place above the critical threshold of $\mathcal{G}^{\text{crit}} = 1.21$, corresponding to uniaxial stretches of 10% (Beauchenne et al., 1989). We restrict the maximum area growth to $\mathcal{G}^{\max} = 4.0$, and assume an adaptation speed of $\tau = 1/12$ and growth exponents of $\gamma = 2.0$ and $\gamma = 12.0$ in Examples 3.1 and 3.2. Sensitivity analyses demonstrate that the parameters τ and γ influence the adaptation time and the shape of the adaptation curve, but not the final state of biological equilibrium (Himpel et al., 2005; Zöllner et al., in press).

3.1. Model problem: Skin growth in equi-biaxial extension

We illustrate the conceptual features of our growth model by exploring the simple model problem of displacement-driven skin expansion of a square $1.0 \times 1.0 \times 0.2$ sheet. In an equi-biaxial setting, we increase the prescribed displacements such that the in-plane area stretch is increased from $\mathcal{G} = 1.0$ to 2.0, 3.0, and 4.0, indicated through the vertical dashed lines in Fig. 3. This implies that the skin sheet is gradually stretched to a final size of 2.0×2.0 , i.e., to four times its original size. After applying the deformation, we allow the tissue to adapt, and recover its homeostatic equilibrium state. After three load increments, we remove the applied stretch and allow the tissue to relax.

Fig. 3 illustrates the resulting temporal evolution of the total area stretch \mathcal{G} , the reversible elastic area stretch \mathcal{G}^e , and the irreversible area growth \mathcal{G}^g . The horizontal dashed lines represent the elastic stretch limit $\mathcal{G}^{\text{crit}}$ beyond which skin growth is activated, and the maximum area growth \mathcal{G}^{\max} . The curves confirm that, at all times, the multiplicative decomposition of the deformation gradient $F = F^e \cdot F^g$ introduced in Eq. (1) carries over to the multiplicative decomposition of the total area stretch $\mathcal{G} = \mathcal{G}^e \mathcal{G}^g$ of Eq. (3). Convergence toward the homeostatic state manifests itself through a gradual increase of growth \mathcal{G}^g at a constant total stretch \mathcal{G} , while the elastic stretch \mathcal{G}^e , and,

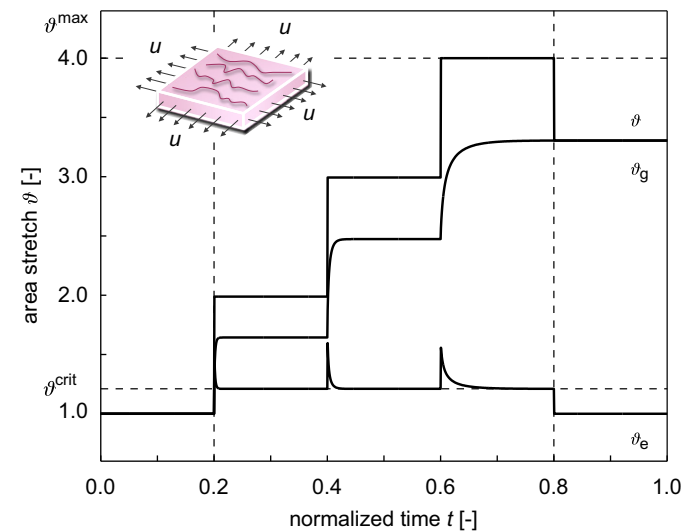


Fig. 3. Temporal evolution of total area stretch \mathcal{G} , reversible elastic area stretch \mathcal{G}^e , and irreversible growth area stretch \mathcal{G}^g for displacement-driven skin expansion. Displacements are increased and then held constant in three intervals between the vertical dashed lines, and then relaxed. Displacement control induces relaxation indicated through the gradual decrease in elastic stretch \mathcal{G}^e and stress, while the growth stretch \mathcal{G}^g increases at a constant total stretch \mathcal{G} . Horizontal dashed lines represent the elastic stretch limit beyond which skin growth is activated $\mathcal{G}^{\text{crit}}$, and the maximum area growth \mathcal{G}^{\max} .

accordingly the stresses, decrease. Upon removal of the applied displacements, the elastic stretch instantaneously returns to its baseline value of one, $\mathcal{G}^e = 1$. Since the growth process is assumed to be irreversible, the growth stretch remains constant, $\mathcal{G}^g = \text{const}$. The total stretch instantaneously adapts the value of the growth stretch, $\mathcal{G} = \mathcal{G}^g$.

Fig. 4 shows the temporal evolution of the skin thickness. Upon loading, the thickness decreases acutely from 1.0 to 0.72, but then returns chronically to its loaded baseline value of 0.88. This value, indicated through the lower horizontal line, is slightly smaller than the original thickness because of the Poisson effect. Upon removal of the applied displacements, the skin thickness immediately returns to its original value of $t=1.0$, indicated through the upper horizontal line. Since the model assumes no growth in thickness direction, $t^g = 1.0$, all thickness changes are fully reversible, $t^e = t$.

3.2. Clinical problem: Skin growth in pediatric forehead reconstruction

To illustrate the full potential of our model, we simulate skin expansion in pediatric forehead reconstruction for two clinical cases, a one-year-old girl in case study I (Gosain and Cortes, 2007), and a one-year-old boy in case study II (Gosain et al., 2009), both born with giant congenital nevi affecting almost half of their foreheads, see Fig. 5. Because giant congenital nevi place the child at an increased risk of skin cancer, the nevus is typically removed in the early childhood (Gosain et al., 2001). To reconstruct the defect, preserve function, and maintain esthetic appearance, both children underwent controlled tissue expansion (LoGiudice and Gosain, 2003). To simulate the process of tissue expansion in an anatomically exact geometry, we create a finite element mesh from three-dimensional computer tomography images of a child of similar age following the procedure outlined in Zöllner et al. (in press). We identify the skin region by its distinct gray scale value in the computer tomography scans to create a triangular surface mesh, which we further smoothen semi-manually. From the smoothened surface mesh, we create a volume mesh of the skin



Fig. 5. Skin expansion in pediatric forehead reconstruction. The patients, a one-year-old girl, case study I shown in the top row (Gosain and Cortes, 2007), and a one-year-old boy, case study II shown in the bottom row (Gosain et al., 2009), both presented with a giant congenital nevus. Three forehead, scalp, and cheek expanders were implanted simultaneously for *in situ* skin growth. After enough skin is grown, the nevus is removed and the new skin is pulled over the wound to close it.

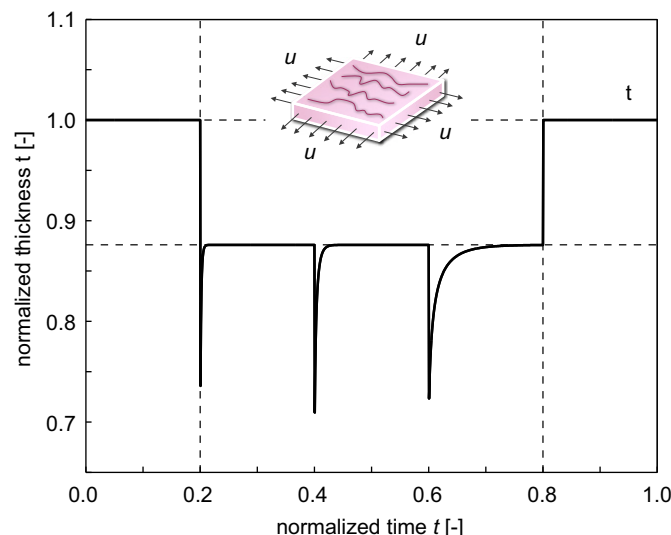


Fig. 4. Temporal evolution of skin thickness t for displacement-driven skin expansion. Displacements are increased and then held constant in three intervals between the vertical dashed lines, and then relaxed. Upon stretching, the skin thickness decreases acutely to 0.72, but then returns chronically to the homeostatic equilibrium thickness of 0.88 indicated through the lower horizontal line. This value is smaller than the original thickness because of the Poisson effect. Upon displacement relaxation, however, the skin thickness immediately returns to its original value of 1.0, indicated through the upper horizontal line.

layer, discretized with 61,228 nodes, 183,684 degrees of freedom, and 30,889 tri-linear brick elements. Last, we assign each element a skin plane normal \mathbf{n}_0 , corresponding to the normal of the initial surface mesh.

Case study I: Simultaneous forehead, anterior and posterior scalp expansion. The first case study mimics the case of a one-year-old girl, whose nevus covered her left posterior forehead (Gosain and Cortes, 2007). To grow extra skin to cover the defect area, she underwent simultaneous tissue expansion in the forehead and in the anterior and posterior scalp as shown in Fig. 5, top row. To model her case, we virtually implant three expanders. First, we implant an expander in the posterior scalp, discretized with 4726 nodes, 14,178 degrees of freedom, and 2270 tri-linear brick elements, covering an initial area of 53.1 cm². Second, we implant two closely connected expanders in the forehead and in the scalp, discretized together with 7954 nodes, 23,862 degrees of freedom, and 3820 tri-linear brick elements, covering an initial area of 96.3 cm². To simulate tissue expansion, we fix all nodes and release only the expander degrees of freedom, which we then pressurize from underneath. We assume that the adjacent dermis and hypodermis remain closely connected (Socci et al., 2007).

Fig. 6 shows the temporal evolution of the normalized total area, elastic area, and growth area upon gradual expander inflation, constant pressure, and gradual expander removal. Once the elastic area stretch reaches the critical threshold of $\mathcal{G}^{\text{crit}} = 1.21$, slightly before the total pressure is applied, at $t=0.125$, the tissue starts to grow. As the expander pressure is held constant, growth increases gradually causing the total area to increase. Then, at $t=0.75$, the pressure is decreased to remove the expander. The elastic area retracts gradually, while the grown area remains constant. The vertical dashed lines correspond to the discrete time points, $t=0.24$, $t=0.33$, $t=0.42$ and $t=0.75$, shown in Fig. 7.

Fig. 7 illustrates the spatio-temporal evolution of the area growth \mathcal{G}^g . Growth is first initiated at the center of the expanders,

where the elastic stretch is largest. As growth spreads throughout the entire expanded areas, the initial area of 149.4 cm² increases gradually as the grown skin area increases to 190.2 cm², 207.4 cm², 220.4 cm², and finally 251.2 cm², shown from left to right. In detail, we observe that the final area in the posterior scalp region is 91.5 cm², corresponding to a fractional area gain of 1.73. In the combined forehead and anterior scalp regions, the final area is 159.6 cm², corresponding to a slightly lower fractional area gain of 1.66. Area growth displays regional variations within $1.0 \leq \vartheta^g \leq 2.0$, i.e., in some regions, the skin has doubled its initial area. Area growth is largest in the center regions and smallest in the peripheries.

Case study II: Simultaneous forehead, scalp, and cheek expansion. The second example mimics the case of a one-year-old boy whose nevus covered his right anterior forehead (Gosain et al., 2009). We simulate his simultaneous tissue expansion with expanders in the forehead, scalp, and cheek as shown in Fig. 5, bottom row. First, we virtually implant an expander in the scalp, discretized with 4356 nodes, 13,068 degrees of freedom, and 2088 tri-linear brick elements, covering an initial area of 50.5 cm². Second, we implant an expander in the cheek, discretized with 2542 nodes,

7626 degrees of freedom, and 1200 tri-linear brick elements, covering an initial area of 29.3 cm². Third, we implant an expander in the forehead, discretized with 3782 nodes, 11,346 degrees of freedom, and 1800 tri-linear brick elements, covering an initial area of 48.8 cm². Again, we fix all nodes and release only the expander degrees of freedom, which we then pressurize from underneath, assuming that the adjacent skin remains unaffected.

Fig. 8 shows the temporal evolution of the normalized total area, elastic area, and growth area upon gradual expander inflation, constant pressure, and gradual expander removal. Similar to Fig. 6, the tissue begins to grow once the elastic area stretch reaches the critical threshold of $\vartheta^{\text{crit}} = 1.21$. Slightly after, at $t = 0.125$, the total pressure is held constant. Similar to the first case study, the skin grows gradually in all three expanded regions. When the pressure is gradually decreased at $t = 0.75$, the elastic area retracts, while the grown area remains constant. The vertical dashed lines correspond to the discrete time points, $t = 0.24$, $t = 0.33$, $t = 0.42$ and $t = 0.75$, shown in Fig. 9.

Fig. 9 illustrates the spatio-temporal evolution of the area growth ϑ^g . Since area stretches are largest at the center of the expander, growth is first initiated in this region, spreading gradually throughout

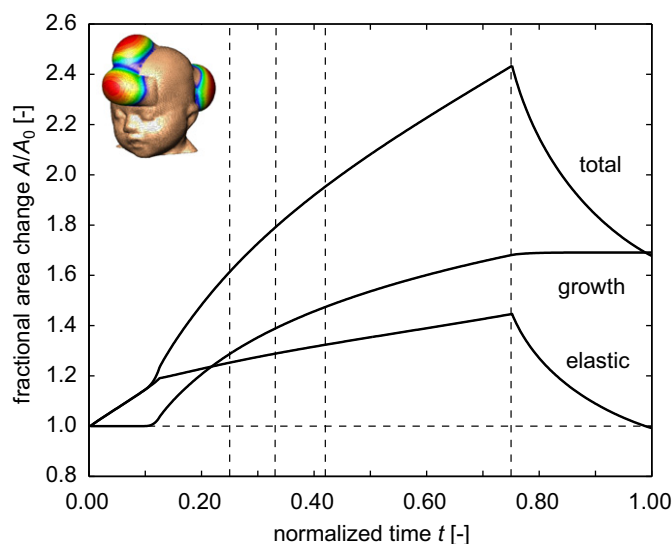


Fig. 6. Skin expansion in pediatric forehead reconstruction. Case study I: Simultaneous forehead, anterior and posterior scalp expansion. Temporal evolution of normalized total area, elastic area, and growth area upon gradual expander inflation, $0.0 < t \leq 0.125$, constant pressure $0.125 < t \leq 0.75$, and deflation $0.75 < t \leq 1.0$. The expanded area increases from 149.4 cm² to 251.2 cm², corresponding to a final fractional area gain of 1.68. Vertical dashed lines correspond to the time points shown in Fig. 7.

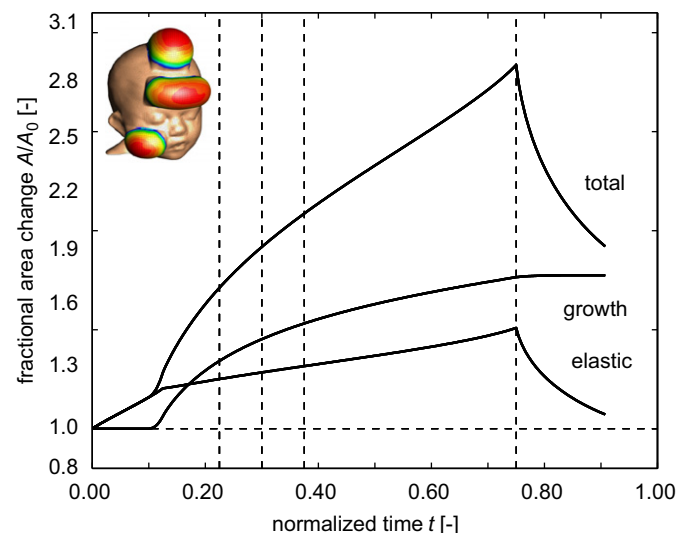


Fig. 8. Skin expansion in pediatric forehead reconstruction. Case study II: Simultaneous forehead, scalp, and cheek expansion. Temporal evolution of normalized total area, elastic area, and growth area upon gradual expander inflation, $0.0 < t \leq 0.125$, constant pressure $0.125 < t \leq 0.75$, and deflation $0.75 < t \leq 1.0$. The expanded area increases from 128.7 cm² to 227.1 cm², corresponding to a final fractional area gain of 1.77. Vertical dashed lines correspond to the time points shown in Fig. 9.

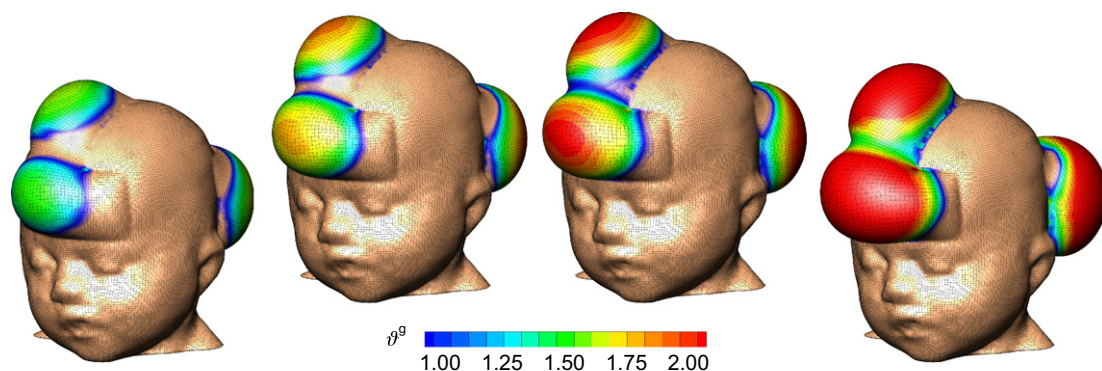


Fig. 7. Skin expansion in pediatric forehead reconstruction. Case study I: Simultaneous forehead, anterior and posterior scalp expansion. Spatio-temporal evolution of area growth displayed at $t = 0.24$, $t = 0.33$, $t = 0.42$ and $t = 0.75$. The initial area of 149.4 cm² increases gradually as the grown skin area increases to 190.2 cm², 207.4 cm², 220.4 cm², and finally 251.2 cm², from left to right.

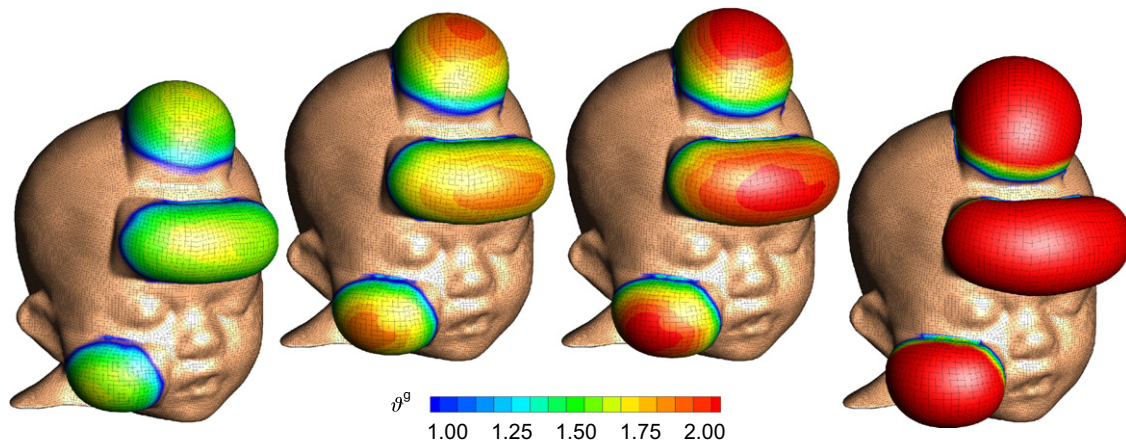


Fig. 9. Skin expansion in pediatric forehead reconstruction. Case study II: Simultaneous forehead, scalp, and cheek expansion. Spatio-temporal evolution of area growth displayed at $t=0.24$, $t=0.33$, $t=0.42$ and $t=0.75$. The initial area of 128.7 cm^2 increases gradually as the grown skin area increases to 176.0 cm^2 , 191.3 cm^2 , 202.1 cm^2 , and finally 227.1 cm^2 , from left to right.

the entire expanded areas. During the growth process, the initial area of 128.7 cm^2 increases to 176.0 cm^2 , 191.3 cm^2 , 202.1 cm^2 , and finally 227.1 cm^2 , shown from left to right. In detail, we observe that the new area in the scalp is 87.9 cm^2 with a fractional area gain of 1.74, in the cheek it is 50.6 cm^2 with a fractional area gain of 1.72, and in the forehead it is 88.6 cm^2 with the largest fractional area gain of 1.82. The area growth varies locally within the range of $1.0 \leq g^g \leq 2.0$ with largest values in the center regions, where skin typically more than doubles its initial area.

4. Discussion

Motivated by the mechanotransduction pathways outlined in Section 1, we have introduced a continuum model for growing skin in response to chronic mechanical overstretch. From a kinematic point of view, the model is based on the multiplicative decomposition of the deformation gradient into an elastic part and a growth part (Rodriguez et al., 1994). From a constitutive point of view, it introduces four material parameters with a clear physiological interpretation (Lubarda and Hoger, 2002; Zöllner et al., in press), the critical physiological stretch limit g^{crit} , the maximum area growth g^{max} , the adaptation speed τ , and the shape of the adaptation curve γ . From a computational point of view, the model is embedded in a standard nonlinear finite element framework, in which the area growth g^g is introduced locally as an internal variable on the integration point level (Himpel et al., 2005; Kuhl et al., 2007). From an algorithmic point of view, the biological equilibrium problem for this internal variable is solved using a local Newton iteration embedded in a global Newton iteration to solve the mechanical equilibrium problem (Göktepe et al., 2010a; Rausch et al., 2011). Overall, our growth model is unconditionally stable, robust, efficient, conceptually modular, and easily portable. In contrast to the only other skin growth model by other authors, which is based on a rotationally symmetric formulation (Socci et al., 2007), our model is conceptually generic, and can handle arbitrary skin geometries. In contrast to our own first prototype of the model, which is based on a material formulation (Buganza Tepole et al., 2011; Zöllner et al., in press), the new realization based on a spatial formulation is computationally elegant and efficient, reducing simulation times by approximately factor five.

In Section 3.1, we have demonstrated the conceptual characteristics of our growth model by means of a simple model problem of successive equi-biaxial extension. Upon displacement

control, the model predicts the following features: (i) an acute increase in the elastic area stretch g^e , (ii) an acute decrease in thickness t , (iii) a chronic increase in area growth g^g , (iv) a chronic restoration of the homeostatic elastic area stretch $g^e \rightarrow g^{\text{crit}}$, and (v) a chronic restoration of the homeostatic equilibrium thickness t . Upon displacement relaxation, the model predicts the following features: (vi) an acute retraction of the elastic area stretch back to its baseline value of $g^e = 1.0$ and (vii) an acute arrest of further growth with $g = g^g = \text{const}$, see Figs. 3 and 4.

Our in silico predictions are in excellent agreement with the in vivo findings reported in the literature. More than three decades ago, the first experimental studies confirmed a net gain in skin area upon tissue expansion (Austad et al., 1982a,b). Unexpectedly, this area gain was found to take place upon conservation of cellular morphology, preservation of phenotype, and maintenance of functionality, without an inflammatory response, and without evidence of malignant degeneration (Beauchenne et al., 1989). This suggested that the increase in tissue surface area is a result of new tissue being regenerated, instead of being recruited from neighboring regions (De Filippo and Atala, 2002). It supports our fundamental model assumption that skin is capable to chronically increase its area, represented through Eq. (3), upon mechanical overstretch, incorporated through Eq. (12), see Fig. 3.

In what follows, we will compare the response of our model to skin growth experiments in the literature (Austad et al., 1982b; Baker, 1991; Beauchenne et al., 1989; van der Kolk et al., 1987; van Rappard et al., 1988; Wollina et al., 1992). Unfortunately, almost all existing data are based on in vivo tissue expansion studies. For the lack of experimental data, we assume that the in vivo strain state of a pressurized thin membrane is close to our in silico state of equi-biaxial extension. Alternatively, we could simulate the true state of tissue expansion using finite element models (Buganza Tepole et al., 2011, in press). However, since this would introduce additional discretization and modeling errors, we will assume a homogeneous strain state here, and focus on comparing the constitutive, material point response.

4.1. Discussion of acute elastic response

Acutely, tissue expansion has been associated with slight epidermal thickening and significant dermal thinning (Austad et al., 1982b), resulting in an overall thinning and a reduced tensile strength (Baker, 1991). Mechanically, a study in rodents reported an acute increase in uniaxial stretch of approximately 36% (Beauchenne et al., 1989). This is in nice agreement with our

model, which predicts an acute elastic area stretch of 1.52, 1.60, and 1.56, corresponding to an average increase in uniaxial stretch of 25%, see Fig. 3. Structurally, the same study identified an initial acute decrease in skin thickness from $407 \pm 3 \mu\text{m}$ to $317 \pm 4 \mu\text{m}$ corresponding to an acute thickness reduction of 22% (Beauchenne et al., 1989). Again, this is in good quantitative agreement with our model, which predicts an acute average normalized thickness of 0.74, 0.71, and 0.72 corresponding to an acute average thickness decrease of 28%, see Fig. 4. Since these acute thickness changes can be attributed primarily to the Poisson effect, they can be utilized to calibrate the elastic material parameters, in particular Poisson's ratio.

4.2. Discussion of chronic growth response

Chronically, tissue expansion is associated with the gradual restoration of baseline histology, baseline mechanics, and baseline structure (Baker, 1991). Histologically, a comparison of piglet tissue in expanded and non-expanded regions demonstrated a chronic restoration of the number of epidermal cell layers and a chronic restoration of the epidermal thickness (van der Kolk et al., 1987). In addition, immunocytochemistry confirmed that the expanded tissue maintains its phenotypical characteristics and native program of cellular differentiation (Wollina et al., 1992). Mechanically, in a multiple time-point study in rodents, an acutely increased uniaxial stretch of 36% was reduced chronically to approximately 10% 32 days post expansion (Beauchenne et al., 1989). This is in excellent agreement with our model, which predicts an acutely increased uniaxial stretch of 25% and a chronic reduction to 10%, see Fig. 3. A uniaxial stretch of 10% would correspond to an area stretch of $\mathcal{J}^{\text{crit}} = 1.21$. In our model, the model parameter $\mathcal{J}^{\text{crit}}$ takes the interpretation of the physiological threshold value, to which the elastic area stretch tends to return during adaptive skin growth, see Eq. (12). Structurally, after an initial acute thickness decrease of 22%, the same study reports a chronic restoration of the homeostatic equilibrium thickness from initially $425 \pm 4 \mu\text{m}$ to $398 \pm 3 \mu\text{m}$, corresponding to a chronic thickness reduction of 7% (Beauchenne et al., 1989). This agrees well with our model, which predicts a normalized homeostatic equilibrium thickness of 0.88, corresponding to a chronic thickness reduction 12%, see Fig. 4. The chronic rodent study also reported that the overall weight of the tissue sample almost tripled, with a fractional weight gain of approximately 2.7 for wet weight and 3.3 for dry weight (Beauchenne et al., 1989). In our model, the fractional weight gain is directly proportional to the fractional area gain of $\mathcal{J}^{\text{S}} = 3.3$ which agrees nicely with these experimental findings, see Fig. 3. Finally, the study found a conservation of the mechanical properties, for example, a constant breaking strength acutely right after expansion and chronically long term (Beauchenne et al., 1989). These findings support our model assumption that ultimately, the newly created skin will have the same microstructure, density, and stiffness, as the original, native tissue (Buganza Tepole et al., 2011, in press).

4.3. Discussion of elastic retraction

Acutely, upon expander removal, an instantaneous retraction of the elastic deformation significantly reduces the overall skin area. In controlled in vivo experiments in pigs, the ratio between the reversible elastic deformation to irreversible growth was almost 2:1 (van Rappard et al., 1988). Since our model assumes that the overall deformation gradient can be multiplicatively decomposed into an elastic and growth part, represented through Eq. (1), it is perfectly capable of reproducing the effect of elastic retraction upon expander removal, see Figs. 3, 6, and 8.

4.4. Discussion of growth heterogeneity

Figs. 7 and 9 clearly indicate the heterogeneity of the growth process with larger values in the center region and smaller values in the periphery. This is in agreement with in vivo studies, which report a fractional area gain of 3.14, i.e., 50% above average, in the center region, and 2.06, i.e., 25% below average, in the periphery (Beauchenne et al., 1989). The authors hypothesized that larger strains in the center region would trigger larger growth. This is in agreement with our model in Eq. (10), where the evolution of area growth is directly correlated to the amount of overstretch through the growth criterion defined in Eq. (12).

4.5. Limitations

Although we have presented both qualitative and quantitative comparisons of the proposed model with acute and chronic tissue expansion experiments from the literature, several limitations remain. First and foremost, the most challenging aspect would be to tie the growth law in Eq. (4) more closely to the underlying mechanobiology described in detail in the introduction section. Comparative gene expression assays and immunohistochemistry of grown versus ungrown tissue samples could help to identify the mechanisms that trigger skin growth on the molecular and cellular level. Similar approaches have been proposed for amelogenesis (Cox, 2010) and tumorigenesis (Astani and Preziosi, 2009; Preziosi and Tosin, 2009) in the past and could also be adopted here. Ideally, this would help to specify our evolution equation for the growth tensor (4) in terms of discrete mechanotransduction cascades through selected extracellular and intracellular events. To this end, we are currently designing a test setup to stretch and grow explanted tissue samples ex vivo. Since most existing data sets on skin growth are based on in vivo measurements of inflated membranes, an ex vivo setting will allow us to create well-defined geometries and boundary conditions such as the equi-biaxial extension test suggested here.

Second, since our goal was to focus primarily on the kinematic characterization of the growth process, the constitutive modeling of the elastic baseline properties of skin has played a minor role. However, the proposed model is inherently modular and the incorporation of more sophisticated constitutive models (Verdier et al., 2009) is relatively straightforward. A typical candidate is a multiple-constituent anisotropic skin model with in-plane anisotropy introduced through a pronounced stiffness along Langer's lines (Kuhl et al., 2005, 2006), which we have successfully combined with the proposed growth model in the past (Buganza Tepole et al., in press). In addition, the growth process itself could be modeled as anisotropic (Göktepe et al., 2010b), e.g., attributed to a pronounced growth along specific microstructural directions. Similarly, through the deposition of large bundles of compacted immature collagen (Baker, 1991; Kroon and Holzapfel, 2007), the underlying collagen network could reorient itself, e.g., to align with the maximum principal strains (Himpel et al., 2008; Kuhl and Holzapfel, 2007). Here, we model growth as a strain-driven process. This implies that the elastic material parameters, or, accordingly, the corresponding stresses, play a less important role than in stress-driven growth, e.g., in hypertension (Kuhl et al., 2007; Rausch et al., 2011). In other words, when using the same model with different Lamé constants or different constitutive models, we would require different expander pressures to obtain the same deformation pattern, but the growth process itself would still be affected by kinematical quantities only. Along the same lines, we have assumed that the effects of resting tension and residual stress are negligible. Both play a critical role when studying instabilities and buckling (Goriely and Ben Amar, 2005; Vandiver and Goriely, 2009). In a previous study, we have

explored these phenomena in more detail (Buganza Tepole et al., 2011). Within the context of finite deformations, resting tension and residual stress could be incorporated through another second order tensor, which would mimic the mapping to a pre-strained or residually stressed configuration (Menzel, 2007; Taber and Humphrey, 2001).

Third, for the sake of simplicity, we have modeled skin as homogeneous across the thickness, neglecting its individual layers and their potential interaction. We are currently refining our model utilizing shell kinematics with a higher resolution across the thickness direction. This will facilitate to model the individual skin layers (Silver et al., 2003), which we believe to be a major source of heterogeneities and residual stresses in real tissue expansion cases (Menzel, 2005). Alternatively, to explore the biomechanical interaction between the growing dermis and the underlying hypodermis during tissue expansion, we could even model growing skin through its own boundary energy (Javili and Steinmann, 2010).

Fourth, at this stage, the chronic response of our model is not yet calibrated in time. We have assumed that chronic growth takes place within a normalized time interval from zero to one. In reality, growth periods range from the order of days in rodents (Beauchenne et al., 1989) to weeks in pigs (van Rappard et al., 1988) and humans (Gosain et al., 2009). However, with the appropriate experimental data, the duration of the adaptation process can be calibrated easily through the adaptation speed τ (Zöllner et al., in press).

Fifth, we have modeled the tissue expander only implicitly through controlling the expander pressure. In real tissue expansion, the external control parameter is the expander volume (LoGiudice and Gosain, 2003). This implies that our simulation displays creep under constant loading, while clinical tissue expansion might rather display relaxation under constant deformation (Buganza Tepole et al., in press). Moreover, we have assumed that the expander is connected tightly to the expanded tissue, neglecting effects of interface sliding and shear (Socci et al., 2007). However, this seems to be a reasonable first assumption, since most current expanders have well-designed textures to promote mild tissue in-growth, primarily to prevent expander migration (Barone et al., 1992).

Last, while our computational model seems well suited to provide qualitative guidelines and trends, in its present state, it is not recommended for quantitative statements. We will need to perform acute and chronic in vitro and in vivo experiments to truly identify the underlying mechanisms which have, up until now, only been represented phenomenologically. Nevertheless, we believe that using the equations of nonlinear continuum mechanics to characterize skin growth represents a significant advancement over the current gold standard to predict tissue growth exclusively in terms of areas, volumes, and empiric correction factors (Shively, 1986; van Rappard et al., 1988).

5. Conclusion

We have presented a continuum model for growing biological membranes in which the underlying mechanobiology is collectively summarized in a single phenomenological internal variable, the in-plane area growth. The model can reliably predict the characteristic histological, mechanical, and structural features of controlled overstretch-induced skin growth, both acutely and chronically. We anticipate that the proposed skin growth model can be generalized to arbitrary biological membranes, and that it can serve as a valuable tool to virtually manipulate membrane area simply by means of changes in the mechanical environment.

Acknowledgments

We acknowledge the support by Professor Arun K. Gosain, Department of Plastic Surgery, Case Western Reserve University, Cleveland, Ohio, for stimulating discussions, and for providing the computer tomography images of the pediatric skulls. This work was supported by the Stanford Graduate Fellowship to Adrián Buganza Tepole and by the National Science Foundation CAREER award CMMI-0952021 and the National Institutes of Health Grant U54 GM072970 to Ellen Kuhl.

References

- Agache, P.G., Monneur, C., Leveque, J.L., DeRigal, J., 1980. Mechanical properties and Young's modulus of human skin in vivo. *Arch. Dermatol. Res.* 269, 221–232.
- Ambrosi, D., Mollica, F., 2002. On the mechanics of a growing tumor. *Int. J. Eng. Sci.* 40, 1297–1316.
- Ambrosi, D., Preziosi, L., Vitale, G., 2010. The insight of mixtures theory for growth and remodeling. *Z. Angew. Math. Phys.* 61, 177–191.
- Ambrosi, D., Ateshian, G.A., Arruda, E.M., Cowin, S.C., Dumaïs, J., Goriely, A., Holzapfel, G.A., Humphrey, J.D., Kerkemer, R., Kuhl, E., Olberding, J.E., Taber, L.A., Garikipati, K., 2011. Perspectives on biological growth and remodeling. *J. Mech. Phys. Solids* 59, 863–883.
- Argenta, L.C., Watanabe, M.J., Grabb, W.C., 1983. The use of tissue expansion in head and neck reconstruction. *Ann. Plast. Surg.* 11, 31–37.
- Arneja, J.S., Gosain, A.K., 2007. Giant congenital melanocytic nevi. *Plast. Reconstr. Surg.* 120, 26e–40e.
- Astanin, S., Preziosi, L., 2009. Mathematical modelling of the Warburg effect in tumour cords. *J. Theor. Biol.* 258, 578–590.
- Austad, E.D., Pasyk, K.A., McClatchey, K.D., Cheery, G.W., 1982a. Histomorphologic evaluation of guinea pig skin and soft tissue after controlled tissue expansion. *Plast. Reconstr. Surg.* 70, 704–710.
- Austad, E.D., Thomas, S.B., Pasyk, K.A., 1982b. Tissue expansion: divided or loan? *Plast. Reconstr. Surg.* 78, 63–67.
- Baker, S.R., 1991. Fundamentals of expanded tissue. *Head Neck* 13, 327–333.
- Barone, F.E., Perry, L., Keller, T., Maxwell, G.P., 1992. The biomechanical and histopathologic effect of surface texturing with silicone and polyurethane in tissue implantation and expansion. *Plast. Reconstr. Surg.* 90, 77–86.
- Beauchenne, J.G., Chambers, M.M., Peterson, A.E., Scott, P.G., 1989. Biochemical, biomechanical, and physical changes in the skin in an experimental animal model of therapeutic tissue expansion. *J. Surg. Res.* 47, 507–514.
- Buganza Tepole, A., Ploch, C.J., Wong, J., Gosain, A.K., Kuhl, E., 2011. Growin skin: a computational model for skin expansion in reconstructive surgery. *J. Mech. Phys. Solids* 59, 2177–2190.
- Buganza Tepole, A., Gosain, A.K., Kuhl, E. Stretching skin: the physiological limit and beyond. *Int. J. Nonlin. Mech.*, doi:10.1016/j.jnonlinmec.2011.07.006, in press.
- Ciarletta, P., Ben Amar, M. Papillary networks in the dermal–epidermal junction of skin: a biomechanical model. *Mech. Res. Commun.*, doi:10.1016/j.mechrescom.2011.12.001, in press.
- Cox, B., 2010. A multi-scale, discrete-cell simulation of organogenesis: application to the effects of strain stimulus on collective cell behavior during ameloblast migration. *J. Theor. Biol.* 262, 58–72.
- De Filippo, R.E., Atala, A., 2002. Stretch and growth: the molecular and physiologic influences of tissue expansion. *Plast. Reconstr. Surg.* 109, 2450–2462.
- Epstein, M., Maugin, G.A., 2000. Thermomechanics of volumetric growth in uniform bodies. *Int. J. Plasticity* 16, 951–978.
- Garikipati, K., 2009. The kinematics of biological growth. *Appl. Mech. Rev.* 62, 030801.1–030801.7.
- Göktepe, S., Abilez, O.J., Parker, K.K., Kuhl, E., 2010a. A multiscale model for eccentric and concentric cardiac growth through sarcomerogenesis. *J. Theor. Biol.* 265, 433–442.
- Göktepe, S., Abilez, O.J., Kuhl, E., 2010b. A generic approach towards finite growth with examples of athlete's heart, cardiac dilation, and cardiac wall thickening. *J. Mech. Phys. Solids* 58, 1661–1680.
- Goriely, A., Tabor, M., 2003. Biomechanical models of hyphal growth in actinomycetes. *J. Theor. Biol.* 222, 211–218.
- Goriely, A., Ben Amar, M., 2005. Differential growth and instability in elastic shells. *Phys. Rev. Lett.* 94, 198103.
- Goriely, A., Ben Amar, M., 2007. On the definition and modeling of incremental, cumulative, and continuous growth laws in morphoelasticity. *Biomech. Model. Mechanobiol.* 6, 289–296.
- Gosain, A.K., Santoro, T.D., Larson, D.L., Gingrass, R.P., 2001. Giant congenital nevi: a 20-year experience and an algorithm for their management. *Plast. Reconstr. Surg.* 108, 622–636.
- Gosain, A.K., Cortes, W., 2007. Pediatric tissue expansion for forehead reconstruction: a 13-year review and an algorithm for its use. *Am. Soc. Plast. Surg. Baltimore, Abstract* 13288.

- Gosain, A.K., Zochowski, C.G., Cortes, W., 2009. Refinements of tissue expansion for pediatric forehead reconstruction: a 13-year experience. *Plast. Reconstr. Surg.* 124, 1559–1570.
- Himpel, G., Kuhl, E., Menzel, A., Steinmann, P., 2005. Computational modeling of isotropic multiplicative growth. *Comput. Model. Eng. Sci.* 8, 119–134.
- Himpel, G., Menzel, A., Kuhl, E., Steinmann, P., 2008. Time-dependent fiber reorientation of transversely isotropic continua—finite element formulation and consistent linearization. *Int. J. Num. Meth. Eng.* 73, 1413–1433.
- Humphrey, J., 2002. *Cardiovascular Tissue Mechanics: Cells, Tissues and Organs*. Springer.
- Jaalouk, D.E., Lammerding, J., 2009. Mechanotransduction gone awry. *Nat. Rev. Mol. Cell Biol.* 10, 63–73.
- Javili, A., Steinmann, P., 2010. On the thermodynamics of solids with boundary structures. *Int. J. Solids Struct.* 47, 3245–3253.
- Kroon, M., Holzapfel, G.A., 2007. A model for saccular cerebral aneurysm growth by collagen fibre remodelling. *J. Theor. Biol.* 247, 775–787.
- Kroon, W., Delhaas, T., Arts, T., Bovendeerd, P., 2009. Computational modeling of volumetric soft tissue growth: application to the cardiac left ventricle. *Biomech. Model. Mechanobiol.* 8, 301–309.
- Kuhl, E., Garikipati, K., Arruda, E.M., Grosh, K., 2005. Remodeling of biological tissue: mechanically induced reorientation of a transversely isotropic chain network. *J. Mech. Phys. Solids* 53, 1552–1573.
- Kuhl, E., Menzel, A., Garikipati, K., 2006. On the convexity of transversely isotropic chain network models. *Philos. Mag.* 86, 3241–3258.
- Kuhl, E., Maas, R., Himpel, G., Menzel, A., 2007. Computational modeling of arterial wall growth: attempts towards patient-specific simulations based on computer tomography. *Biomech. Model. Mechanobiol.* 6, 321–331.
- Kuhl, E., Holzapfel, G.A., 2007. A continuum model for remodeling in living structures. *J. Mater. Sci.* 2, 8811–8823.
- Langevin, H.M., Bouffard, N.A., Badger, G.J., Iatridis, J.C., Howe, A.K., 2005. Dynamic fibroblast cytoskeletal response to subcutaneous tissue stretch ex vivo and in vivo. *Am. J. Physiol. Cell Physiol.* 288, C747–C756.
- Lee, E.H., 1969. Elastic–plastic deformation at finite strains. *J. Appl. Mech.* 36, 1–6.
- LoGiudice, J., Gosain, A.K., 2003. Pediatric tissue expansion: indications and complications. *J. Craniofac. Surg.* 14, 866–872.
- Lubarda, A., Hoger, A., 2002. On the mechanics of solids with a growing mass. *Int. J. Solids Struct.* 39, 4627–4664.
- Lubarda, V.A., 2004. Constitutive theories based on the multiplicative decomposition of deformation gradient: thermoelasticity, elastoplasticity and biomechanics. *Appl. Mech. Rev.* 57, 95–108.
- McMahon, J., Goriely, A., 2010. Spontaneous cavitation in growing elastic membranes. *Math. Mech. Solids* 15, 57–77.
- Menzel, A., 2005. Modelling of anisotropic growth in biological tissues—a new approach and computational aspects. *Biomech. Model. Mechanobiol.* 3, 147–171.
- Menzel, A., 2007. A fibre reorientation model for orthotropic multiplicative growth. *Biomech. Model. Mechanobiol.* 6, 303–320.
- Neumann, C.G., 1959. The expansion of an area of skin by progressive distension of a subcutaneous balloon; use of the method for securing skin for subtotal reconstruction of the ear. *Plast. Reconstr. Surg.* 19, 124–130.
- Preziosi, L., Tosin, A.R., 2009. Multiphase modelling of tumour growth and extracellular matrix interaction: mathematical tools and applications. *J. Math. Biol.* 58, 625–656.
- Radovan, C., 1982. Breast reconstruction after mastectomy using the temporary expander. *Plast. Reconstr. Surg.* 69, 195–208.
- Rausch, M.K., Dam, A., Göktepe, S., Abilez, O.J., Kuhl, E., 2011. Computational modeling of growth: systemic and pulmonary hypertension in the heart. *Biomech. Model. Mechanobiol.* 10, 799–811.
- Rivera, R., LoGiudice, J., Gosain, A.K., 2005. Tissue expansion in pediatric patients. *Clin. Plast. Surg.* 32, 35–44.
- Rodriguez, E.K., Hoger, A., McCulloch, A.D., 1994. Stress-dependent finite growth in soft elastic tissues. *J. Biomech.* 27, 455–467.
- Schmid, H., Pauli, L., Paulus, A., Kuhl, E., Itskov, M., 2011. How to utilise the kinematic constraint of incompressibility for modelling adaptation of soft tissues. *Comput. Methods Biomech. Biomed. Eng.* doi:10.1080/10255842.2010.548325.
- Serup, J., Jemec, G.B.E., Grove, G.L., 2003. *Handbook of Non-invasive Methods and the Skin*. Informa Healthcare.
- Shively, R.E., 1986. Skin expander volume estimator. *Plast. Reconstr. Surg.* 77, 482–483.
- Silver, F.H., Siperko, L.M., Seehra, G.P., 2003. Mechanobiology of force transduction in dermal tissue. *Skin Res. Technol.* 9, 3–23.
- Simpson, C.L., Patel, D.M., Green, K.J., 2011. Deconstructing the skin. *Cytoarchitectural determinants of epidermal morphogenesis. Nat. Rev. Mol. Cell Biol.* 12, 565–580.
- Socci, L., Rennati, G., Gervaso, F., Vena, P., 2007. An axisymmetric computational model of skin expansion and growth. *Biomech. Model. Mechanobiol.* 6, 177–188.
- Taber, L.A., 1995. Biomechanics of growth, remodeling and morphogenesis. *Appl. Mech. Rev.* 48, 487–545.
- Taber, L.A., Eggers, D.W., 1996. Theoretical study of stress-modulated growth in the aorta. *J. Theor. Biol.* 180, 343–357.
- Taber, L.A., Humphrey, J.D., 2001. Stress-modulated growth, residual stress, and vascular heterogeneity. *J. Biomech. Eng.* 123, 528–535.
- Takei, T., Mills, I., Arai, K., Sumpio, B.E., 1998. Molecular basis for tissue expansion: clinical implications for the surgeon. *Plast. Reconstr. Surg.* 102, 247–258.
- Taylor, R.L., 2008. *FEAP—A Finite Element Analysis Program. User Manual, Version 8.2*. University of California, Berkeley.
- van der Kolk, C.A., McCann, J.J., Knight, K.R., O'Brien, B.M., 1987. Some further characteristics of expanded tissue. *Clin. Plast. Surg.* 14, 447–453.
- Vandiver, R., Goriely, A., 2009. Differential growth and residual stress in cylindrical elastic structures. *Philos. Trans. R. Soc. A* 367, 3607–3630.
- van Rappard, J.H.A., Molenaar, J., van Doorn, K., Sonneveld, G.J., Borghouts, J.M.H.M., 1988. Surface-area increase in tissue expansion. *Plast. Reconstr. Surg.* 82, 833–839.
- Verdier, C., Etienne, J., Duperray, A., Preziosi, L., 2009. Review: rheological properties of biological materials. *C. R. Phys.* 10, 790–811.
- Wollina, U., Berger, U., Stolle, C., Stolle, H., Schubert, H., Zieger, M., Hipler, C., Schumann, D., 1992. Tissue expansion in pig skin—a histochemical approach. *Anat. Histol. Embryol.* 21, 101–111.
- Wong, V.W., Akaishi, S., Longaker, M.T., Gurtner, G.C., 2011. Pushing back: wound mechanotransduction in repair and regeneration. *J. Invest. Dermatol.* 131 (11), 2186–2196.
- Zöllner, A.M., Buganza Tepole, A., Gosain, A.K., Kuhl, E., Growing skin—tissue expansion in pediatric forehead reconstruction. *Biomech. Model. Mechanobiol.*, doi:10.1007/s10237-011-0357-4, in press.